International Journal of Minerals, Metallurgy and Materials
Volume 23, Number 10, October 2016, Page 1204
DOI: 10.1007/s12613-016-1340-y

Nanostructured multilayer thin films of multiwalled carbon nanotubes/gold nanoparticles/glutathione for the electrochemical detection of dopamine

Ekarat Detsri[1,2], *Sirilak Rujipornsakul*[1], *Tanapong Treetasayoot*[1], *and Pawarit Siriwattanamethanon*[1]

1) Department of Chemistry, Faculty of Science, King Mongkut's Institute of Technology Ladkrabang, Bangkok 10520, Thailand
2) Advanced Materials Research Unit, Faculty of Science, King Mongkut's Institute of Technology Ladkrabang, Bangkok 10520, Thailand
(Received: 11 February 2016; revised: 19 April 2016; accepted: 30 May 2016)

Abstract: In the present study, multiwalled carbon nanotubes (MWCNTs), gold nanoparticles (AuNPs), and glutathione (GSH) were used to fabricate multilayer nanoscale thin films. The composite thin films were fabricated by layer-by-layer technique as the films were constructed by the alternate deposition of cationic and anionic polyelectrolytes. The MWCNTs were modified via a noncovalent surface modification method using poly(diallydimethylammonium chloride) to form a cationic polyelectrolyte. An anionic polyelectrolyte was prepared by the chemical reduction of $HAuCl_4$ using sodium citrate as both the stabilizing and reducing agent to form anionic AuNPs. GSH was used as an electrocatalyst toward the electro-oxidation of dopamine. The constructed composite electrode exhibits excellent electrocatalytic activity toward dopamine with a short response time and a wide linear range from 1 to 100 μmol/L. The limits of detection and quantitation of dopamine are (0.316 ± 0.081) μmol/L and (1.054 ± 0.081) μmol/L, respectively. The method is satisfactorily applied for the determination of dopamine in plasma and urine samples to obtain the recovery in the range from 97.90% to 105.00%.

Keywords: multiwalled carbon nanotubes; gold; nanoparticles; glutathione; dopamine

1. Introduction

Dopamine is an important catecholamine neurotransmitter in the mammalian renal and central nervous systems [1]. Progressive loss of dopamine is likely to results in the neurodegenerative diseases such as schizophrenia, Alzheimer's disease, and Parkinson's disease [2]. Recently, electrochemical spectroscopy has gained considerable attention for the determination of dopamine. However, problems have arisen with the electrochemical detection of dopamine, such as the interferences from coexisting species of uric acid and ascorbic acid, which may overlap the voltammetric responses at oxidation peak potentials similar to those of dopamine [3]. Thus, the development of modified electrodes for the selective and sensitive detection of dopamine has been a goal of researchers in this area. Modified electrode materials developed for the electrochemical simultaneous detection of dopamine include functionalized carbon-based materials [4–6], metal nanoparticles [7–9], and conducting polymers [10–12]. Among the attractive nanomaterials identified thus far, multiwalled carbon nanotubes (MWCNTs) and gold nanoparticles (AuNPs) have been studied in a wide variety of applications. Special attention has been devoted to MWCNTs because of their stable chemical and physical properties, good thermal stability, high surface area, and high conductivity [13]. AuNPs are mostly used in electrocatalysis because they enable fast electron transfer on the surface of electrodes [14].

Recently, MWCNT multilayer thin films have attracted great interest because of their unique electrical properties [15], which have made them a promising component for the fabrication of electrochemical sensors [16]. Within the last two years, our group has developed an easy procedure to fabricate multilayer thin films of MWCNTs by layer-by-layer (LbL) technique to improve the films' electrical properties [17]. Because MWCNTs cannot be easily dispersed in water or any organic solvent because of van der

Corresponding author: Ekarat Detsri E-mail: Ekarat.de@kmitl.ac.th

Waals interactions between nanotubes, the nanotube–nanotube aggregation tends to occur [18]. The development of efficient methodologies for modifying the surface of MWCNTs is needed to overcome this obstacle. Two main approaches to the surface modification of MWCNTs have been proposed: noncovalent and covalent surface modification [19].

In this work, MWCNTs were modified by noncovalent surface modification using poly(diallydimethylammonium chloride) (PDADMAC). Multilayer thin films of MWCNTs·PDADMAC electrodes were fabricated using the LbL technique. Because our application is based on the MWCNTs' electrical conductivity, AuNPs was deposited onto MWCNT thin films, improving the electrical properties of MWCNTs composite materials. One benefit of AuNP deposition onto MWCNTs was to enhance the electron transfer on the surface of electrodes. Moreover, the electrochemical detection of dopamine was improved by the attachment of glutathione (GSH) to an MWCNTs·PDADMAC/AuNP composite thin-film electrode to enhance the electrode's specific electrocatalytic activity toward dopamine. The optical and electrical properties of MWCNTs·PDADMAC/AuNPs/GSH composite thin-film electrodes were characterized by four-point-probe resistivity measurements and UV–vis spectrophotometry, whereas the surface morphology, thickness, and surface roughness were characterized by field-emission scanning electron microscopy (FESEM) and atomic force microscopy (AFM), respectively.

2. Experimental

2.1. Chemicals and materials

MWCNTs (outer-diameter distribution 6–13 nm; length distribution 2.5–20 μm), dopamine hydrochloride ($C_8H_{11}NO_2$), L-Glutathione ($C_{10}H_{17}N_3O_6S$), poly(sodium 4-styrene sulfonate) (PSS), poly(diallydimethylammonium chloride) (PDADMAC), tetrachloroauric(III) acid trihydrate ($HAuCl_4{\cdot}3H_2O$), and sodium citrate dihydrate ($C_6H_5Na_3O_7$) were purchased from Sigma-Aldrich Co. Ltd., USA. All of the chemicals were used without further purification. All solutions were prepared using double-distilled water with a resistivity of 18 MΩ·cm.

2.2. Noncovalent surface modification of MWCNTs

Prior to the coating of MWCNTs with the polyelectrolyte, PDADMAC was needed to provide the positive charges on the surface of the tubes via noncovalent surface modification. The polyelectrolyte coating improved the MWCNTs' dispersion in water. The dispersion of MWCNTs by PDADMAC was carried out by mixing 5 mg of MWCNTs with different concentrations of PDADMAC (0.001, 0.01, 0.1, 0.5, and 1.0 mmol/L). The mixtures were sonicated using a probe sonicator in an ice bath for 30 min and were subsequently stored at room temperature for 24 h. For each different PDADMAC concentration, the dispersion of MWCNTs was evaluated by UV–vis spectrophotometry at a wavelength of 550 nm.

2.3. Synthesis of AuNPs

AuNPs were prepared using the Turkevich chemical reduction process [20]. The $HAuCl_4{\cdot}3H_2O$ solution was mixed with a sodium citrate solution, and the resulting mixture was boiled and stirred until a red-wine-colored solution was obtained. In our experiments, the aqueous $HAuCl_4{\cdot}3H_2O$ concentration was fixed at 1 mmol/L, whereas the sodium citrate concentration was varied from 10 mmol/L, 20 mmol/L, and 50 mmol/L.

2.4. Fabrication of indium tin oxide (ITO)/(MWCNTs·PDADMAC)/AuNPs/GSH-modified electrodes

The indium tin oxide (ITO) substrate was ultrasonically cleaned with ethanol, acetone, and water, in sequence. To improve the growth of the MWCNTs·PDADMAC, AuNP, and GSH composite thin films, the ITO substrate was coated in an LbL fashion with up to four layers of PDADMAC and PSS to enhance the adhesion between the composite solution and the substrate. The surface, with a top layer of polyanion polymer PSS, was then immersed for 10 min in a solution containing MWCNTs·PDADMAC and subsequently rinsed three times with water. The ITO/MWCNTs·PDADMAC film was then sequentially dipped into 50 mL of AuNP solution to form the desired architecture. Alternating LbL films of MWCNTs·PDADMAC and AuNPs were prepared by repeating this process until the desired number of layers was obtained. The process was then propagated up to nine layers. Finally, the top layer of the MWCNT/AuNP thin films was immersed in 50 mL of 100 mmol/L GSH solution. When completed, the modified electrode was dried with a stream of nitrogen gas and stored in a closed container. The modified electrodes were subsequently denoted as ITO/(MWCNTs·PDADMAC)/AuNPs/GSH.

2.5. Electrochemical measurements

The electrochemical experiments were carried out using three electrodes, including an ITO/(MWCNTs·PDADMAC)/AuNPs/GSH-modified electrode as the working electrode, an Ag/AgCl electrode as the reference electrode, and Pt wire as the counter electrode. Cyclic voltammetry was performed

in the potential range from −0.15 to 0.6 V. The measurements were carried out in a 100 mmol/L phosphate buffer solution (PBS, pH 6.5) at a scan rate of 20 $mV \cdot s^{-1}$ at room temperature.

2.6. Characterization

UV–vis spectra were collected on a double-beam UV–vis spectrophotometer (Shimadzu UV1800, China). A Tecnai T20-G2 transmission electron microscope (FEI, The Netherlands) operated at an accelerating voltage 120 kV was used to observe the dispersion of MWCNTs in the presence of PDADMAC and the size and morphology of the AuNPs; the samples for transmission electron microscopy (TEM) were deposited onto 200-mesh Cu grids coated with Formvar. A NanoZS zetasizer (Malvern Instruments, UK) was used to measure the surface charges of the MWCNTs·PDADMAC and AuNPs. The surface topography and thickness of the multilayer thin films were measured by AFM (NanoScope IV, Veeco Instruments, USA) and FESEM (JSM-7001F, JEOL Solution for Innovation, Germany). The structures of multilayer films were analyzed by X-ray diffraction (XRD) (Bruker D8 Advance, Cu K_α radiation, $20° \leq 2\theta \leq 80°$). The electrochemical experiments were performed using an Autolab PGSTAT302N High Performance (Metrohm, The Netherlands); Pt wire was used as the counter electrode, an Ag/AgCl electrode was used as the reference electrode, and an ITO/(MWCNTs·PDADMAC)/AuNPs/GSH-modified electrode was used as the working electrode.

3. Results and discussion

3.1. Preparation and characterization of ITO/(MWCNTs·PDADMAC)/AuNPs/GSH-modified electrodes

Our main motivation in this work was to use the LbL technique to fabricate the composite (MWCNTs·PDADMAC)/AuNPs/GSH thin-film electrodes for dopamine detection, which were constructed by the alternating deposition of cationic and anionic polyelectrolytes. Cationic MWCNT polyelectrolytes were prepared by noncovalent surface modification using PDADMAC as the dispersing agent. The concentration of PDADMAC strongly affected the dispersion of MWCNTs; therefore, different concentrations of PDADMAC were prepared with MWCNTs. Pristine MWCNTs (5 mg) was dispersed in 100 mL of PDADMAC, and the polymer concentration was varied from 0.001 to 1.0 mmol/L. Fig. 1(a) shows a plot of the change in absorbance of the solution as a function of the added PDADMAC concentration. From the initial solution of aggregated MWCNTs, as the PDADMAC concentration is increased from 0.001 to 0.01 mmol/L, the adsorption of the polymer onto MWCNTs leads to dispersion. The increase in absorbance quickly levels off, suggesting that all of the MWCNTs present in the solution are dispersed. A further increase of the PDADMAC concentration to 0.1 mmol/L does not induce any increase in absorbance. During the dispersion process, intermolecular interactions improve the solubility of MWCNTs in the PDADMAC via the quaternary ammonium group of PDADMAC, which is the most hydrophobic group present in the system and therefore adsorbs and arranges onto the MWCNTs surface [17].

To further confirm that MWCNTs could be dispersed with PDADMAC, TEM was used to investigate the dispersions. The micrograph presented in Fig. 1(a_1) shows that most of the individual nanotubes are uniform compared to the bundle of pristine MWCNTs in Fig. 1(a_2). An interesting point was to determine whether the optimum PDADMAC concentration (0.1 mmol/L) would also be the best condition for the growth of LbL films. Fig. 1(b) shows that the maximum deposition is achieved from a solution prepared with 0.1 mmol/L PDADMAC. Interestingly, when the PDADMAC concentration is increased, the absorbance of film decreases. It was hypothesized that the high PDADMAC content led to a competition phenomenon [17]. To characterize the electrical properties of MWCNTs·PDADMAC multilayer films, the electrical conductivity of each prepared film was characterized using four-point-probe measurements, as shown in Fig. 1(c). These results show that the conductivity of the MWCNTs·PDADMAC multilayer thin films reaches a maximum when prepared from 0.1 mmol/L PDADMAC at the dispersion step.

Anionic AuNPs were prepared by the reduction of $HAuCl_4$ in the presence of sodium citrate, where sodium citrate acted as both a reducing and stabilizing agent. The ability of sodium citrate to stabilize AuNPs was studied by varying the sodium citrate concentration from 10 mmol/L, 20 mmol/L, and 50 mmol/L while fixing the $HAuCl_4$ concentration at 1 mmol/L. As shown in Fig. 2, the plasmon absorption spectra are observed at 520–535 nm, and the peaks in this region are usually assumed to indicate AuNPs [21]. The particle sizes of AuNPs observed by TEM in Figs. 2(a_1)–(a_3) decrease with increasing amount of sodium citrate. Previous studies [21] have demonstrated that the progressive addition of $HAuCl_4$ to a concentrated solution of sodium citrate leads to a decrease of the average particle size of the AuNPs. To investigate the effect of the particle size of AuNPs on the electrical properties of films, the LbL technique was used to prepare multilayers of AuNP thin films

via the deposition of five layers of PDADMAC and AuNPs prepared from various concentrations of sodium citrate in the feed solution. Fig. 2(a_4) shows the electrical properties of the glass slide coated with five layers of AuNPs stabilized with sodium citrate. These results demonstrate that the films assembled from solutions with lower sodium citrate concentrations exhibit the highest electrical conductivity. The increase in the conductivity of AuNPs might be due to the low electrostatic repulsion and low charge density of the stabilizer. The low concentration of sodium citrate generated the dense packing because of the weak repulsive force among particles.

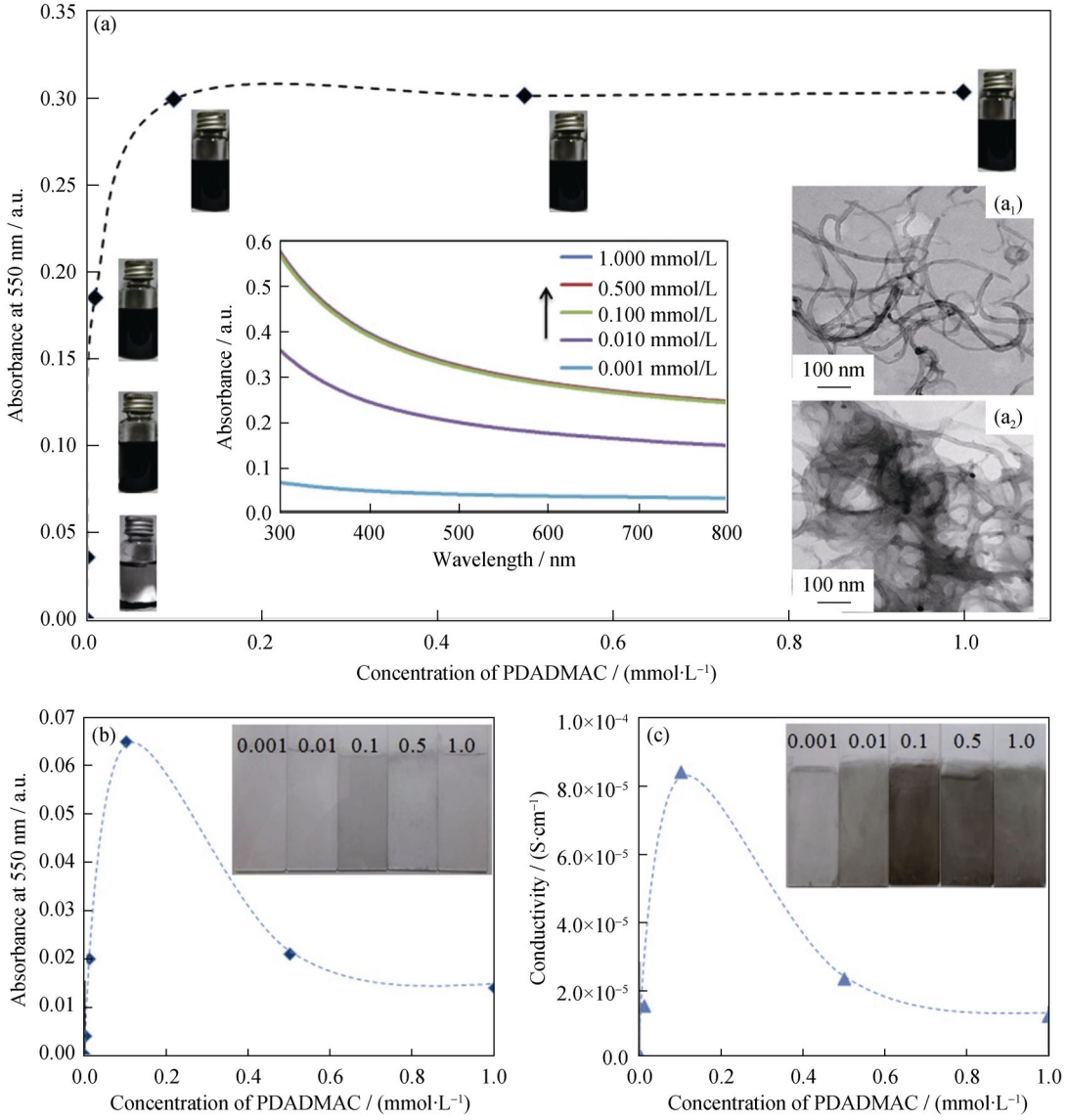

Fig. 1. Effect of PDADMAC concentration on the dispersion of MWCNTs (a) and representative TEM images of MWCNTs dispersed with 0.1 mmol/L PDADMAC (a_1) and pristine MWCNTs (a_2), change in absorbance of a glass slide coated with a monolayer of MWCNTs·PDADMAC as a function of PDADMAC concentration in the dispersion of MWCNTs (b), and conductivity of 10-layer MWCNT·PDADMAC/PSS multilayer thin films at various PDADMAC concentrations in the dispersion of MWCNTs (c).

To confirm the successful dispersion of MWCNTs in the presence of PDADMAC and AuNPs stabilized by sodium citrate, FTIR was used to analyze the functional groups of each compound. Fig. 3 shows the FTIR spectra of pristine MWCNTs, PDADMAC, and MWCNTs dispersed with PDADMAC. The FTIR spectrum of PDADMAC shows characteristic peaks at 1191 cm^{-1} and 1510 cm^{-1}; these peaks correspond to the C–N stretching and C–H bending vibrations of quaternary ammonium groups, respectively. In the FTIR spectra of pristine MWCNTs, no absorption peaks are observed over the investigated wavelength range. By contrast, characteristic absorbance peaks of both PDADMAC and pristine MWCNTs are observed in the FTIR spectra of MWCNTs dispersed with PDADMAC. The main

peaks associated with quaternary ammonium groups are observed at 1190 cm^{-1} and 1510 cm^{-1} in the FTIR spectra, demonstrating that the MWCNTs are dispersed. Figs. 3(d) and (e) show the plots of FTIR spectra of sodium citrate and AuNPs stabilized by sodium citrate, respectively. The FTIR spectrum of sodium citrate shows characteristic peaks at 1416 cm^{-1} and 1693 cm^{-1} for the C–O and C=O stretching vibrations of carboxylic groups, respectively. All characteristic absorbance peaks of sodium citrate are also observed in the FTIR spectra of AuNPs stabilized by sodium citrate.

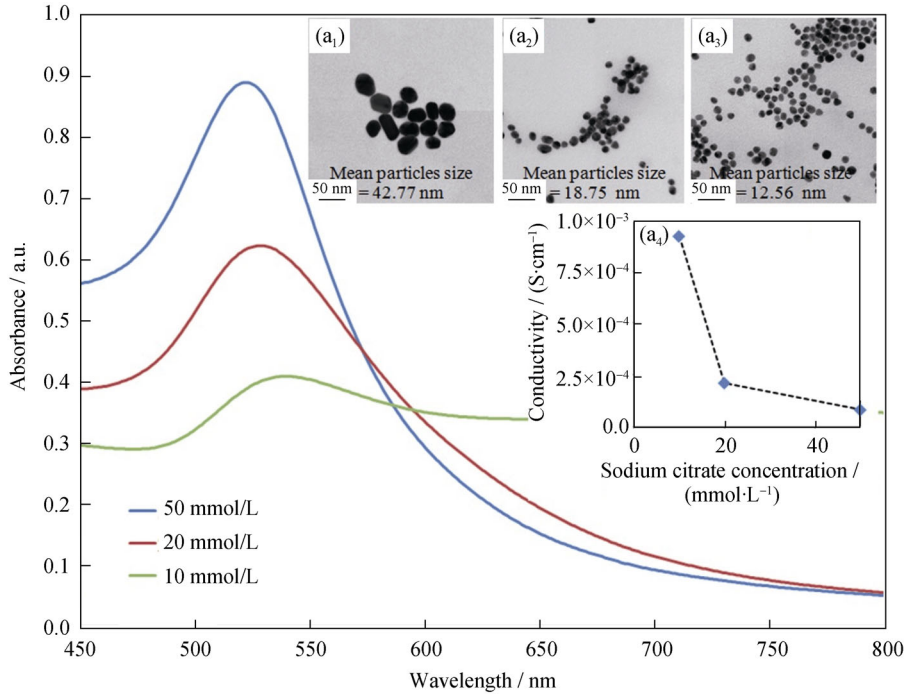

Fig. 2. Absorption spectra of AuNPs prepared using different concentrations of sodium citrate, where the insets are the TEM images of AuNPs with 10:1 (a_1), 20:1 (a_2), and 50:1 (a_3) Na_3Ct:$HAuCl_4$ concentration ratios, and electrical conductivity of AuNP multilayer thin films at five layers (a_4).

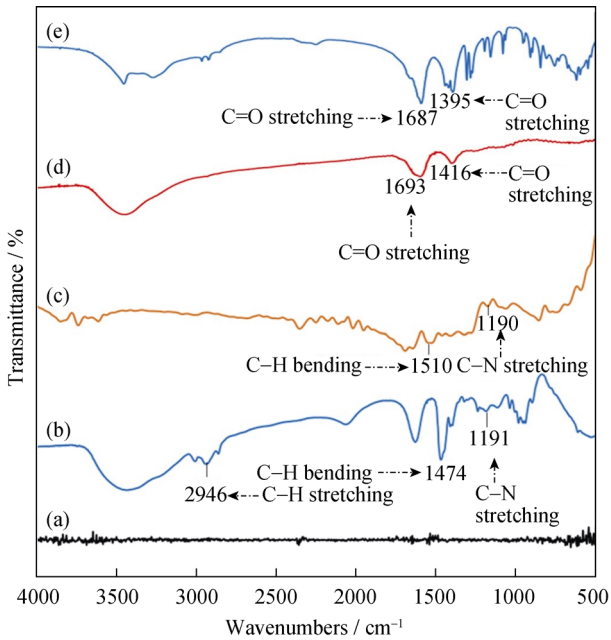

Fig. 3. FTIR spectra of pristine MWCNTs (a), PDADMAC (b), MWCNTs·PDADMAC (c), sodium citrate (d), and AuNPs stabilized with sodium citrate (e).

The goal of this work was to deposit anionic AuNPs and cationic MWCNTs into composite thin films using the LbL technique. The main driving force in the construction of composite thin films was the electrostatic interaction between anionic AuNPs stabilized with sodium citrate and cationic MWCNTs dispersed with PDADMAC. The surface charges of anionic AuNPs and cationic MWCNTs could be estimated via the measurements of zeta potential. The anionic AuNPs and cationic MWCNTs were observed to have zeta potentials of (−32.36 ± 0.05) mV and (53.96 ± 0.01) mV, respectively. UV–vis spectrophotometry and AFM were used to monitor the growth of composite thin films as a function of the number of layers. The multilayer of anionic AuNPs and cationic MWCNT composite thin films is shown in Fig. 4. The increase in absorbance and thickness are constant for each deposition step because the amount of materials being deposited for each dipping cycle is constant. The electrical conductivity of the prepared composite thin films is presented in the inset of Fig. 4, which shows that the electrical conductivity increases with increasing number of

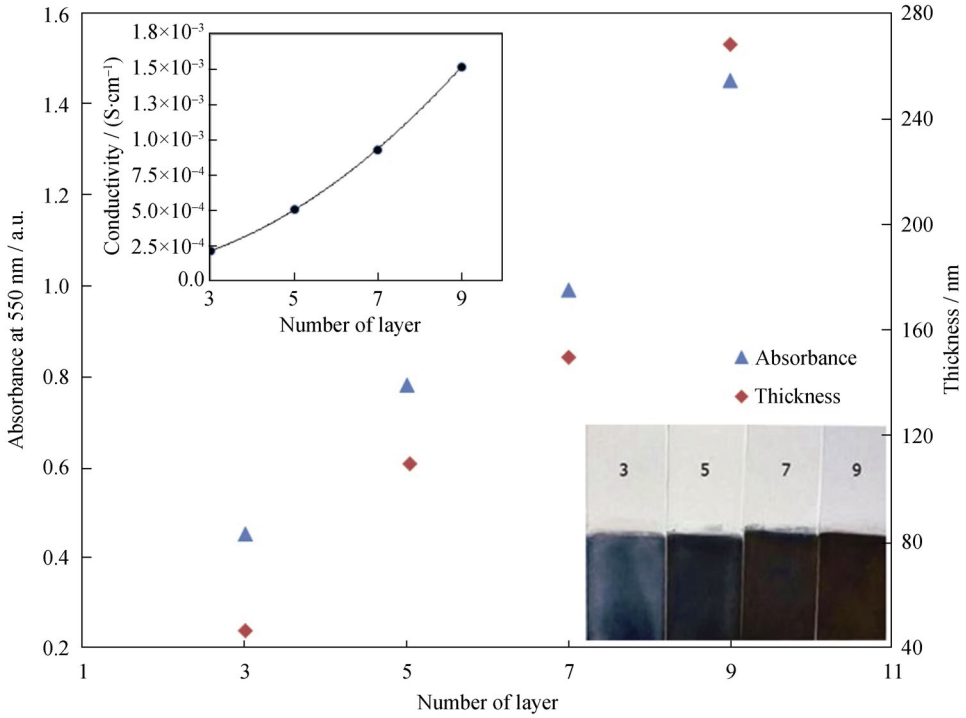

Fig. 4. Thickness, absorbance, and conductivity values as a function of the number of layers of (MWCNTs·PDADMAC)/AuNP multilayer films and representative digital images of assembled (MWCNTs·PDADMAC)/AuNP multilayer films.

layers. On the basis of the four-point-probe measurements, the composite thin films with nine layers are identified as exhibiting the best conductivity among the grown thin films.

The surface topography of MWCNTs·PDADMAC and AuNP composite thin films as functions of the number of layers is shown in Fig. 5. The amounts of MWCNTs and AuNPs in the composite films are increased by increasing the number of layers. The nanoparticles are densely packed onto the films' surface, where they exhibit an interconnection network structure, as observed in the FESEM images in Fig. 6. The LbL films exhibit the separated individual MWCNTs because of the electrostatic repulsion between nanotubes that act against van der Waals interactions that yield the close-packed aggregates; the electrostatic cross-linking between cationic MWCNTs and anionic AuNPs during the LbL process also contributes to the aggregate formation. This aggregate formation leads to randomly oriented, kinetically driven MWCNT and AuNP arrangements in the films. The root-mean-square (RMS) roughness values determined from AFM images at 3, 5, 7, and 9 layers are (91.92 ± 1.37), (101.12 ± 1.21), (128.39 ± 1.53), and (304.02 ± 1.74) nm, respectively.

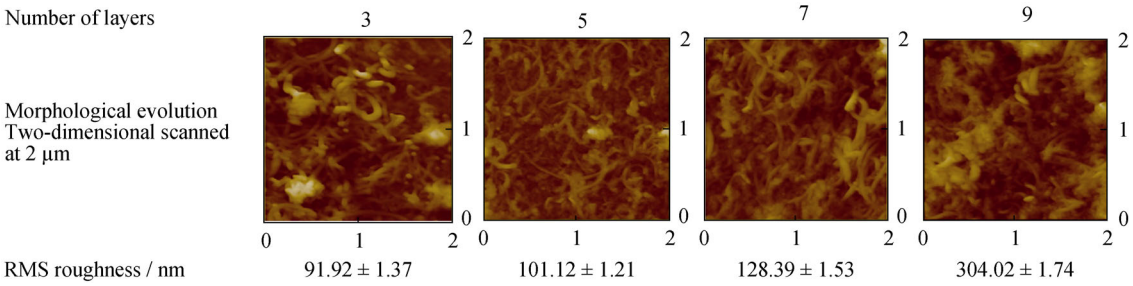

Fig. 5. AFM images of assembled (MWCNTs·PDADMAC)/AuNPs/GSH multilayer films.

To confirm the growth of the MWCNT and AuNP composites, XRD was used to analyze the crystalline structure of the composite thin films. The XRD pattern of pristine MWCNTs is shown in Fig. 7(a). Prominent peaks in the XRD pattern of pristine MWCNTs are observed at 25.90° and 42.70°, representing the [002] and [100] reflections of carbon, respectively. In Fig. 7(b), the XRD patterns of the AuNP thin films exhibit the identical characteristic [111], [200], [220], and [311] reflections at 38.50°, 44.36°, 64.73°, and 77.63°, respectively, representing the diffraction planes

of the cubic structure of Au metal. All of the characteristic reflections of pristine MWCNTs and AuNPs are observed in the XRD pattern of MWCNTs·PDADMAC and AuNP composite thin films (Fig. 7(c)), demonstrating the successful fabrication of composite thin films using the LbL technique.

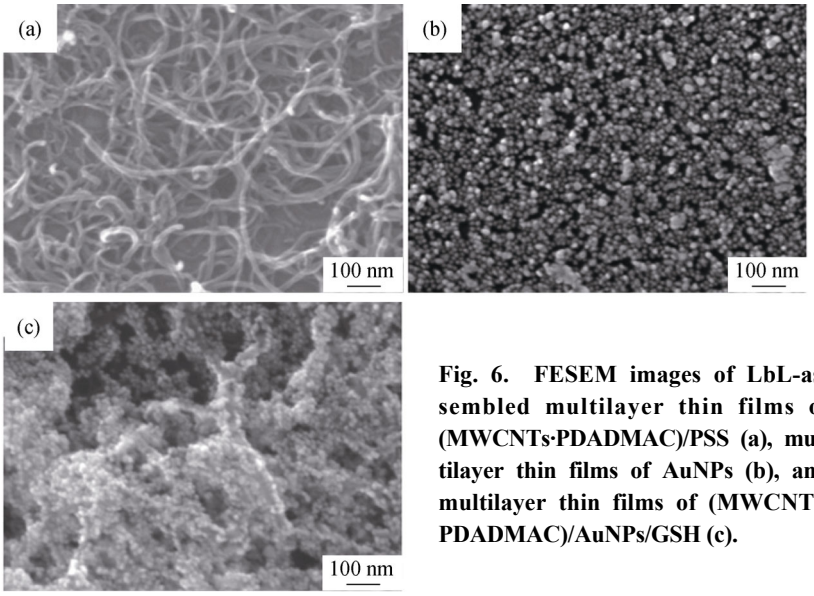

Fig. 6. FESEM images of LbL-assembled multilayer thin films of (MWCNTs·PDADMAC)/PSS (a), multilayer thin films of AuNPs (b), and multilayer thin films of (MWCNTs·PDADMAC)/AuNPs/GSH (c).

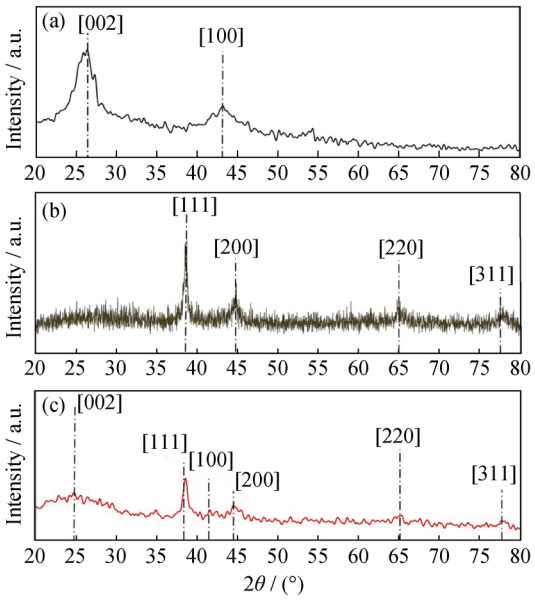

Fig. 7. XRD patterns of pristine MWCNTs (a), multilayer films of AuNPs (b), and multilayer films of (MWCNTs·PDADMAC)/AuNPs/GSH (c).

GSH was used as an electrocatalyst toward the electro-oxidation of dopamine. The LbL technique was used to pattern GSH molecules onto the top layer of MWCNTs·PDADMAC/AuNP composite thin films. The nine layers of negatively charged MWCNTs·PDADMAC/AuNP composite thin films were immersed in a GSH solution at pH 7.00. The adsorption of GSH at the thin-film interface was controlled by a diffusion process. Time played a major role in the formation of a multilayer. The occurrence of high deposition at pH 7.00 was due to the high positively charged density of the GSH solution. The amine group of cysteine in GSH was completely ionized at pH 8.75 or less [22] and could act as a cationic polyelectrolyte for film assembly.

3.2. Electrochemical detection of dopamine using ITO/(MWCNTs·PDADMAC)/AuNPs/GSH-modified electrodes

Fig. 8 displays a representative schematic of dopamine electrochemical oxidation at an ITO/(MWCNTs·PDADMAC)/AuNPs/GSH-modified electrode. The free carboxylic groups of GSH enhanced the electrostatic interaction between the negatively charged electrode and positively charged dopamine molecules. Dopamine was electrochemically oxidized into dopamine-*o*-quinone, resulting in the improved selectivity and sensitivity of the ITO/(MWCNTs·PDADMAC)/AuNPs/GSH-modified electrodes toward dopamine.

To investigate the ability of the ITO/(MWCNTs·PDADMAC)/AuNPs/GSH-modified electrodes to detect dopamine, the cyclic voltammograms of 200 μmol/L dopamine were recorded in 0.1 mol/L PBS buffer solutions at different pH levels. The electrochemical behavior of dopamine also included the transfer of protons, consistent with previous reports [23–25]. The voltammograms in Fig. 9 show that the oxidation peak potential of dopamine shifts toward the negative potentials with increasing pH value, suggesting that dopamine oxidation involves a two-proton and two-electron process [26]. The oxidation peak current (I_p) of dopamine reaches a maximum at pH 6.5.

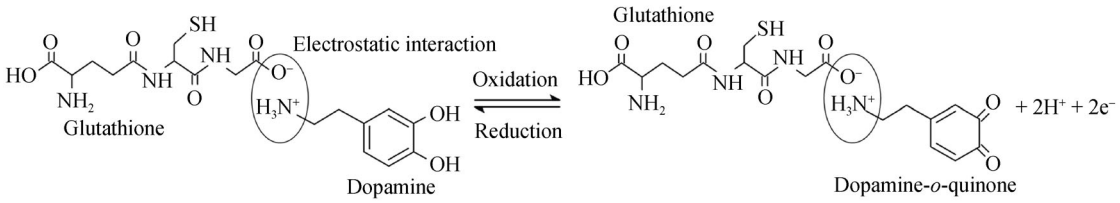

Fig. 8. Ttypical electro-oxidation mechanism of dopamine at an ITO(MWCNTs·PDADMAC)/AuNPs/GSH-modified electrode.

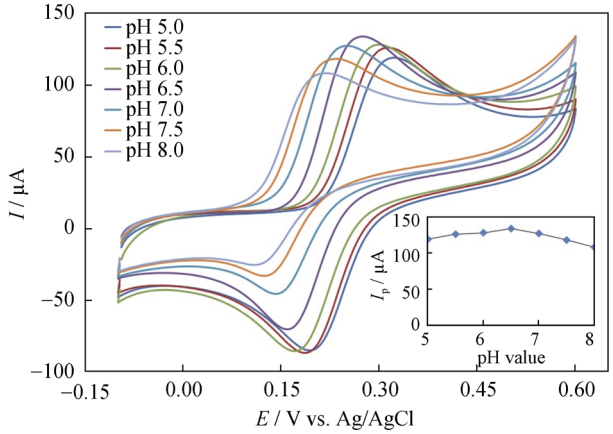

Fig. 9. Cyclic voltammograms of 200 μmol/L dopamine at different pH levels (pH 5–pH 8), as collected using the ITO/(MWCNTs·PDADMAC)/AuNPs/GSH-modified electrode at the scan rate of 20 mV·s^{-1}.

To elucidate the kinetics of electrode reaction, the effect of scan rate (V) on the electrochemical behavior of dopamine was investigated. Fig. 10 shows the cyclic voltammograms of 200 μmol/L dopamine in pH 6.5 PBS buffer solution at various scan rates (10–100 mV·s^{-1}) on an ITO/(MWCNTs·PDADMAC)/AuNPs/GSH-modified electrode. The oxidation peak current (I_p) is observed to increase with increasing scan rate. The plot of I_p as a function of $V^{1/2}$ in the range from 10 to 100 mV·s^{-1} results in a linear-regression equation as $I_p = 52.029V^{1/2} - 104.01$; the plot shows an excellent linear relationship ($R^2 = 0.995$). The modified electrode exhibits the good electrochemical determination of dopamine in the scan-rate range from 10 to 100 mV·s^{-1}, suggesting that the electrode potential is controlled by the diffusion process.

Fig. 11 presents the electrochemical response of ITO/(MWCNTs·PDADMAC)/AuNPs/GSH-modified electrodes to different concentrations of dopamine ($C_{Dopamine}$, 10–100 μmol/L). The oxidation peak currents are observed to increase with increasing dopamine concentration. The corresponding linear-regression equation for dopamine is expressed as $I_{anode} = 0.779C_{Dopamine} + 9.013$, with a correlation coefficient of 0.9983. Therefore, the results demonstrated that the modified electrode was stable for dopamine detection when used as an electrochemical sensor. The limit of detection (LOD, 3SD/slope of calibration) and limit of quantitation (LOQ, 10SD/slope of calibration) were (0.316 ± 0.081) μmol/L and (1.054 ± 0.081) μmol/L, respectively, which were substantially better than those of the previous modified electrode, as summarized in Table 1.

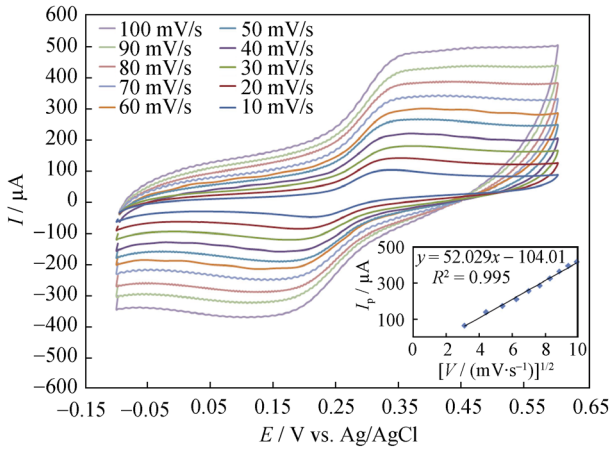

Fig. 10. Cyclic voltammograms of 20 μmol/L dopamine at various scan rates (10–100 mV·s^{-1}) and oxidation peak current vs. scan rate.

The ITO/(MWCNTs·PDADMAC)/AuNPs/GSH-modified electrode was used to detect dopamine in the presence of KCl, $C_6H_{12}O_6$, $CaCO_3$, uric acid, ascorbic acid, and citric acid. The effects of interfering substances were tested by mixing 200 μmol/L dopamine with the maximum concentration of each interfering species in biological fluids. Fig. 12 presents the electrochemical oxidation peaks obtained with an electrode modified to function in the presence of dopamine and interfering species. According to the results, KCl, $C_6H_{12}O_6$, $CaCO_3$, uric acid, ascorbic acid, and citric acid do not interfere with the determination of dopamine. The oxidation current of all mixed solutions of dopamine and interfering species are observed to have the same oxidation current as dopamine, demonstrating its high selectivity detection.

The stability and repeatability of the ITO/(MWCNTs·PDADMAC)/AuNPs/GSH-modified electrodes for the detection of dopamine were investigated through a number of cycles. The results in Fig. 13 for the determination of 200 μmol/L dopamine in 0.1 mol/L PBS buffer solution were

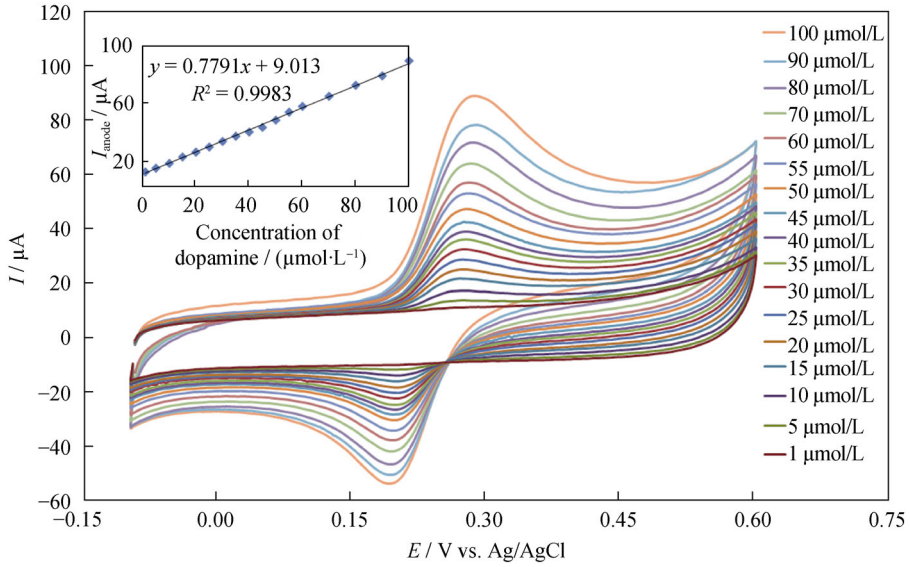

Fig. 11. Cyclic voltammograms of various concentrations of dopamine (1–100 μmol/L) on an ITO/(MWCNTs·PDADMAC)/AuNPs/GSH-modified electrode.

Table 1. Performance comparison of different modified electrodes for the detection of dopamine.

Electrode materials	pH value	Scan rate / ($mV \cdot s^{-1}$)	Dynamic range / ($\mu mol \cdot L^{-1}$)	Limit of detection / ($\mu mol \cdot L^{-1}$)	Reference
Carbon paste electrode/Rhodamine B	7.0	5	6–1000	3.99	[27]
Carbon paste electrode/SDS micelles	7.0	80	8–134	3.70	[28]
Carbon paste electrode/PBD-MWCNTs	7.0	100	30–800	1.00	[29]
Carbon paste electrode/Horseradish peroxidase immobilized on PEGylated polyurethane nanoparticles	6.5	100	17–1900	2.00	[30]
Glassy carbon electrode/MWCNTs	8.0	50	3–200	0.80	[31]
Carbon paste electrode/L-arginine	5.6	50	50–100	0.50	[32]
ITO/MWCNT·PDADMAC/AuNPs/GSH	6.5	20	1–100	0.316	This work

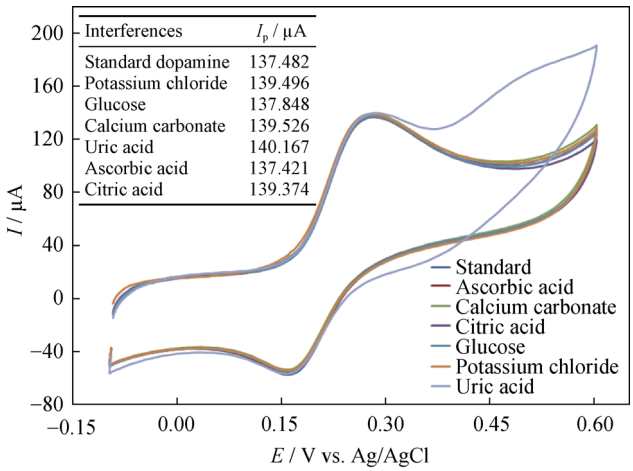

Fig. 12. Effect of coexisting substances on the detection of dopamine, where the inset is the oxidation peak current of 100 μmol/L coexisting substance mixed with 100 μmol/L dopamine solution on an ITO/(MWCNTs·PDADMAC)/AuNPs/GSH-modified electrode.

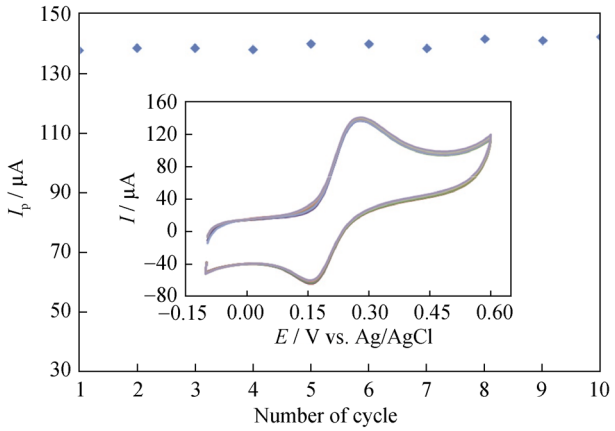

Fig. 13. Reproducibility of the cyclic voltammetric responses of an ITO/(MWCNTs·PDADMAC)/AuNPs/GSH-modified electrode in 100 μmol/L dopamine solution containing 0.1 mol/L PBS (pH 6.5).

observed to have good stability and repeatability, with a relative standard deviation (RSD) of 0.45% after the same

modified electrode is used ten times; thus, this electrode is attractive for use in pharmaceutical electrochemical sensors.

Table 2 shows the cyclic voltammetric responses of an ITO/(MWCNTs·PDADMAC)/AuNPs/GSH-modified electrode for the determination of dopamine in real samples. Biological fluids such as plasma and urine were used for analysis of dopamine using the method of standard additions. The results show that the recovery of the plasma samples ranges from 97.90% to 110.00% for plasma samples, with an RSD of 0.75%–1.48%. By contrast, the recovery of urine samples ranges from 96.10% to 105.00%, with an RSD of 1.09%–3.49%. These results demonstrated that an ITO/(MWCNTs·PDADMAC)/AuNPs/GSH-modified electrode could be an appropriate choice for the simultaneous determination of dopamine in biological samples.

Table 2. Determination results for dopamine in real samples

Samples	Concentration of dopamine / ($\mu mol \cdot L^{-1}$)		Recovery / %	RSD / %
	Added	Found		
Plasma	0	Not detected	—	—
	1	1.10 ± 0.01	110.0	1.48
	5	4.89 ± 0.03	97.9	0.75
	10	10.04 ± 0.02	100.4	1.87
	30	29.94 ± 0.01	99.8	0.81
	50	50.40 ± 0.02	100.8	0.98
Urine	0	Not detected	—	—
	1	1.05 ± 0.01	105.0	3.04
	5	4.80 ± 0.01	96.1	3.49
	10	10.16 ± 0.02	101.6	0.85
	30	29.92 ± 0.01	99.7	1.27
	50	50.51 ± 0.03	101.0	1.09

4. Conclusions

In this work, the LbL deposition technique was successfully used to fabricate a composite electrode of MWCNTs, AuNPs, and GSH for the determination of dopamine using the cyclic voltammetry technique. The composite electrode was prepared by electrostatic interaction of the cationic MWCNTs dispersed with PDADMAC and the anionic AuNPs. The positively charged GSH was used as an electrocatalyst toward the electro-oxidation of dopamine. The modified composite electrode exhibits the high efficiency in dopamine detection, with the excellent stability and reproducibility. This new information related to the ITO/(MWCNTs·PDADMAC)/AuNPs/GSH-modified electrode prepared by LbL technique can be of great interest for the determination of dopamine in biological fluids and in the pharmaceutical industry.

Acknowledgements

This work was financially supported by the Faculty of Science, King Mongkut's Institute of Technology Ladkrabang, Bangkok, Thailand (No. 2558-02050067).

References

[1] A.H. Liu, I. Honma, and H.S. Zhou, Amperometric biosensor based on tyrosinase-conjugated polysaccharide hybrid film: Selective determination of nanomolar neurotransmitters metabolite of 3,4-dihydroxyphenylacetic acid (DOPAC) in biological fluid, *Biosens. Bioelectron.*, 21(2005), No. 5, p. 809.

[2] J.W. Mo and B. Ogorevc, Simultaneous measurement of dopamine and ascorbate at their physiological levels using voltammetric microprobe based on overoxidized poly(1,2-phenylenediamine)-coated carbon fiber, *Anal. Chem*., 73(2001), No. 6, p. 1196.

[3] M.A. Dayton, A.G. Ewing, and R.M. Wightman, Response of microvoltammetric electrodes to homogeneous catalytic and slow heterogeneous charge-transfer reactions, *Anal. Chem*., 52(1980), No. 14, p. 2392.

[4] K.J. Huang, Q.S. Jing, Z.W. Wu, L. Wang, and C.Y. Wei, Enhanced sensing of dopamine in the present of ascorbic acid based on graphene/poly(*p*-aminobenzoic acid) composite film, *Colloids Surf. B*, 88(2011), No. 1, p. 310.

[5] X.G. Liu, Y.H. Peng, X.J. Qu, S.Y. Ai, R.X. Han, and X.B. Zhu, Multi-walled carbon nanotube-chitosan/poly(amidoamine)/DNA nanocomposite modified gold electrode for determination of dopamine and uric acid under coexistence of ascorbic acid, *J. Electroanal. Chem.*, 654(2011), No. 1-2, p. 72.

[6] S. Sainio, T. Palomäki, S. Rhode, M. Kauppila, O. Pitkänen, T. Selkälä, G. Toth, M. Moram, K. Kordas, J. Koskinen, and T. Laurila, Carbon nanotube (CNT) forest grown on diamond-like carbon (DLC) thin films significantly improves electrochemical sensitivity and selectivity towards dopamine, *Sens. Actuators*, *B*, 211(2015), p. 177.

[7] W.Y. Chu, Q. Zhou, S.S. Li, W. Zhao, N. Li, and J.W. Zheng, Oxidation and sensing of ascorbic acid and dopamine on self-assembled gold nanoparticles incorporated within polyaniline film, *Appl. Surf. Sci.*, 353(2015), p. 425.

[8] V. Vinoth, J.J. Wu, A.M. Asiri, and S. Anandan, Simultaneous detection of dopamine and ascorbic acid using silicate network interlinked gold nanoparticles and multi-walled carbon nanotubes, *Sens. Actuators B*, 210(2015), p. 731.

[9] Y.M. Leng, K. Xie, L. Ye, G.Q. Li, Z.W. Lu, and J.B. He, Gold-nanoparticle-based colorimetric array for detection of dopamine in urine and serum, *Talanta*, 139(2015), p. 89.

[10] L. Yang, S. Liu, Q. Zhang, and F. Li, Simultaneous electrochemical determination of dopamine and ascorbic acid using

AuNPs@polyaniline core–shell nanocomposites modified electrode, *Talanta*, 89(2012), p. 136.

[11] A. Stoyanova, S. Ivanov, V. Tsakova, and A. Bund, Au nanoparticle-polyaniline nanocomposite layers obtained through layer-by-layer adsorption for the simultaneous determination of dopamine and uric acid, *Electrochim. Acta*, 56(2011), No. 10, p. 3693.

[12] M.U. Anu Prathap and R. Srivastava, Tailoring properties of polyaniline for simultaneous determination of a quaternary mixture of ascorbic acid, dopamine, uric acid, and tryptophan, *Sens. Actuators B*, 177(2013), p. 239.

[13] S. Iijima, Helical microtubules of graphitic carbon, *Nature*, 354(1991), p. 56.

[14] S. Suarasan, M. Focsan, O. Soritau, D. Maniu, and S. Astilean, One-pot, green synthesis of gold nanoparticles by gelatin and investigation of their biological effects on Osteoblast cells, *Colloids Surf. B*, 132(2015), p. 122.

[15] J.P.C. Trigueiro, G.G. Silva, F.V. Pereira, and R.L. Lavall, Layer-by-layer assembled films of multi-walled carbon nanotubes with chitosan and cellulose nanocrystals, *J. Colloid Interface Sci.*, 432(2014), p. 214.

[16] R. Sedghi and Z. Pezeshkian, Fabrication of non-enzymatic glucose sensor based on nanocomposite of MWCNTs-COOH-poly (2-aminothiophenol)-Au NPs, *Sens. Actuators B*, 219(2015), p. 119.

[17] E. Detsri and S.T. Dubas, Layer-by-layer deposition of cationic and anionic carbon nanotubes into thin films with improved electrical properties, *Colloids Surf. A*, 444(2014), p. 89.

[18] C. Iamsamai, A. Soottitantawat, U. Ruktanonchai, S. Hannongbua, and S.T. Dubas, Simple method for the layer-by-layer surface modification of multiwall carbon nanotubes, *Carbon*, 49(2011), No. 6, p. 2039.

[19] C. Iamsamai, S. Hannongbua, U. Ruktanonchai, A. Soottitantawat, and S.T. Dubas, The effect of the degree of deacetylation of chitosan on its dispersion of carbon nanotubes, *Carbon*, 48(2010), No. 1, p. 25.

[20] J. Turkevich, Colloidal gold: Part I. Historical and preparative aspects, morphology and structure, *Gold Bull*, 18(1985), No. 3, p. 86.

[21] X. Ji, X. Song, J. Li, Y. Bai, W. Yang, and X.J. Peng, Size control of gold nanocrystals in citrate reduction: the third role of citrate, *J. Am. Chem. Soc.*, 129(2007), No. 45, p. 13939.

[22] I.S. Lim, D. Mott, W. Ip, P.N. Njoki, Y. Pan, S.Q. Zhou, and C.J. Zhong, Interparticle interactions in glutathione mediated assembly of gold nanoparticles, *Langmuir*, 24(2008), No. 16, p. 8857.

[23] E. Molaakbari, A. Mostafavi, and H. Beitollahi, Simultaneous electrochemical determination of dopamine, melatonin, methionine and caffeine, *Sens. Actuators B*, 208(2015), p. 195.

[24] S.P. Qi, B. Zhao, H.Q. Tang, and X.Q. Jiang, Determination of ascorbic acid, dopamine, and uric acid by a novel electrochemical sensor based on pristine graphene, *Electrochim. Acta*, 161(2015), p. 395.

[25] W.J. Lui, J. Xiao, C.S. Wang, H.Y. Yin, H.F. Xie, and R.S. Cheng, Synthesis of polystyrene-grafted-graphene hybrid and its application in electrochemical sensor of dopamine, *Mater. Lett.*, 100(2013), p. 70.

[26] Z. Temoçin, Modification of glassy carbon electrode in basic medium by electrochemical treatment for simultaneous determination of dopamine, ascorbic acid and uric acid, *Sens. Actuators B*, 176(2013), p. 796.

[27] T. Thomas, R.J. Mascarenhas, and B.E. Kumara Swamy, Poly(Rhodamine B) modified carbon paste electrode for the selective detection of dopamine, *J. Mol. Liq.*, 174(2012), p. 70.

[28] E.C. Orozco, M.T. Ramírez-Silva, S.C. Avendaño, M.R. Romo, and M.P. Pardavé, Electrochemical quantification of dopamine in the presence of ascorbic acid and uric acid using a simple carbon paste electrode modified with SDS micelles at pH 7, *Electrochim. Acta*, 85(2012), p. 307.

[29] M. Mazloum-Ardakani, M. Abolhasani, B. Mirjalili, M.A. Sheikh-Mohseni, A. Dehghani-Firouzabadi, and A. Khoshroo, Electrocatalysis of dopamine in the presence of uric acid and folic acid on modified carbon nanotube paste electrode, *Chin. J. Catal.*, 35(2014), No. 2, p. 201.

[30] M.B. Fritzen-Garcia, F.F. Monteiro, T. Cristofolini, J.J.S. Acuña, B.G. Zanetti-Ramos, I.R.W.Z. Oliveira, V. Soldi, A.A. Pasa, and T.B. Creczynski-Pasa, Characterization of horseradish peroxidase immobilized on PEGylated polyurethane nanoparticles and its application for dopamine detection, *Sens. Actuators B*, 182(2013), p. 264.

[31] Z.A. Alothman, N. Bukhari, S.M. Wabaidur, and S. Haider, Simultaneous electrochemical determination of dopamine and acetaminophen using multiwall carbon nanotubes modified glassy carbon electrode, *Sens. Actuators B*, 146(2010), No. 1, p. 314.

[32] B.N. Chandrashekar, B.E. Kumara Swamy, M. Pandurangachar, T.V. Sathisha, and B.S. Sherigara, Electropolymerisation of L-arginine at carbon paste electrode and its application to the detection of dopamine, ascorbic and uric acid, *Colloids Surf. B*, 88(2011), No. 1, p. 413.